JOURNAL OF THERMOPHYSICS AND HEAT TRANSFER
Vol. 7, No. 4, Oct.–Dec. 1993

Numerical Method for Simulating Fluid-Dynamic and Heat-Transfer Changes in Jet-Engine Injector Feed-Arm Due to Fouling

V. R. Katta*
Systems Research Laboratories, Inc., Dayton, Ohio 45440
and
W. M. Roquemore†
Wright Laboratory, Wright-Patterson Air Force Base, Ohio 45433

A computational method for integrating fluid-dynamic simulations and heat-transfer calculations in different segments of solid boundaries has been developed to predict deposition inside tubes. The fuel thermal-degradation mechanism is treated mathematically using a four-step global-chemistry model. Deposits are allowed to grow on the wall surface, and the resulting fluid-dynamic and heat-transfer changes are implicitly computed using a time-dependent formulation. Turbulent-flow simulations for the fuel flow bounded by the fuel-deposit interface are made on a body-oriented coordinate system. The induction period, which is associated with the slower deposition during the initial hours of exposure, is modeled by introducing a wall-reaction-type mechanism for the surface sticking phenomenon. Calculations are made for full-scale and half-scale gas-turbine injector feed-arm rigs. The temperature at the deposit-tube interface is found to increase with deposition. Computed accumulated deposit weight and changes in the tube-inner-wall temperature with time are compared with the experimental data. The effects of fouling on heat transfer and blockage to the fuel flow are discussed.

Introduction

IN a gas-turbine engine, fuel is fed to the atomizers through the injector feed-arms. Attempts by designers to increase engine performance result in increasing compressor-exit and, thereby, feed-arm temperatures. Bulk-fuel temperatures are also expected to increase in high-performance aircraft due to the higher heat loads which the fuel will experience as it is used to cool the engine lube oil, avionics, environmental systems, and fuel controls.[1] The combination of high fuel-inlet and tube-wall surface temperatures makes the injector feed-arm very susceptible to fouling due to decomposition of the fuel. When fuel degrades and forms insoluble gums and hard carbonaceous deposits, the small apertures in the fuel nozzles and atomizers can become clogged, or fouled, leading to spray-pattern distortions, unscheduled overhauls, and, potentially, engine malfunction.[2] This will constitute a serious problem in future high-speed aircraft.

The thermal stability of jet fuels has been studied for many years, and a considerable quantity of data has been collected under various experimental conditions and for different types of experimental arrangements. However, the overall complexity and a lack of fundamental understanding of the processes leading to fouling have hindered the development of a general theoretical framework which can be used to interpret or predict different types of experimental results. Empirically based fouling models[3,4] are potentially applicable to many engineering problems; however, they cannot be generally applied to different experimental configurations and they do not provide fundamental insight into the deposition processes. Time-averaged computational-fluid-dynamic and chemistry (CFDC) models[5] based on numerical solutions of conservation of mass, momentum, and energy are much more general than empirical models, and can be applied to different test-section geometries over a wide range of test conditions. Thus, the time-averaged CFDC models represent a significant advancement; however, they are most applicable to a thin deposition layer which does not appreciably affect the heat-transfer and fuel-flow characteristics—a limitation which results from these models providing the deposition rate rather than the actual time evolution of deposits in the system.

The real-time evolution of deposits is important in fuel-system components such as the nozzle feed-arm because it can be used to determine the change in performance of a fuel-system component as a function of time. As deposits begin to grow on the tube walls, they offer resistance to the heat flow and block the fuel flow.

A cross section of a typically fouled tube is depicted in Fig. 1. Usually, peak deposition occurs somewhere along the tube, depending on the thermo-fluid-dynamic stressing of the fuel. Wall deposition inside the tube alters the fluid dynamics and heat transfer which, in turn, modify the fuel degradation. The fluid-dynamic changes due to deposition are apparent; however, changes in heat transfer depend on the heating environment. In laboratory experiments which study fouling problems, tubes are often heated by passing electric current through the tube walls. In this case, because of the constant heat flux across the tube wall, the temperature at the outer wall increases with deposition, while that at the fuel-deposit interface (and, hence, that of the fuel) remains more or less undisturbed. Therefore, the chemical kinetics of fuel degradation may not be affected by the accumulation of deposits on the tube wall, which somewhat simplifies the problem. However, the higher temperatures within the deposits chemically alter their morphology, resulting in layers of deposits having different densities[6] which is misrepresented as a change in the rate of deposition. Normally, heating in a fuel-nozzle feed-arm does not take place in this way. These tubes are usually heated with a constant-temperature heat source, and the temperature at the fuel-deposit interface decreases with deposi-

Presented as Paper 92-0768 at the AIAA 30th Aerospace Sciences Meeting and Exhibit, Reno, NV, Jan. 6–9, 1992; received Jan. 31, 1992; revision received Sept. 9, 1992; accepted for publication Sept. 9, 1992.

*Senior Engineer, Research Applications Division, Arvin/Calspan, 2800 Indian Ripple Road. Member AIAA.

†Senior Scientist, Fuels and Lubrication Division, Aero Propulsion and Power Directorate. Member AIAA.

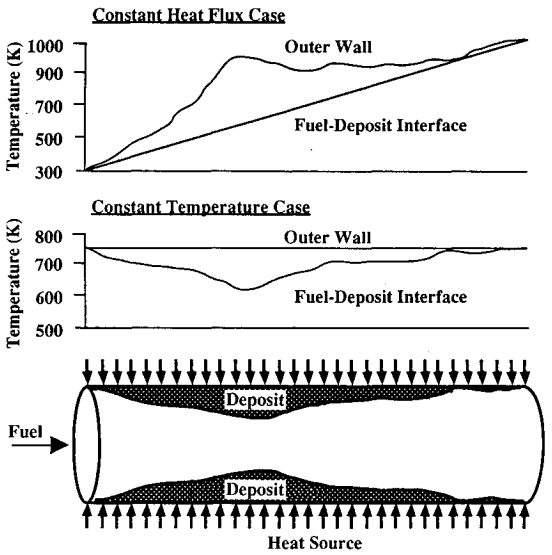

Fig. 1 Effect of deposition on heat transfer in tubes under different heating conditions.

tion. The lower fuel temperature alters the decomposition process inside the tube. A computational technique capable of simulating the time evolution of deposition would be useful in addressing this problem. A time-dependent model[7] was recently developed in this laboratory to predict deposit formation in electrically heated tubes over long periods of time. By varying the deposit density as a function of exposure time, reasonable comparisons between predicted and measured values have been obtained. Since these experiments were conducted under fixed electrical power conditions, the temperature distribution of the fuel did not change with deposition (cf. Fig. 1), simplifying the boundary conditions.

In the present study, a mathematical approach was developed to provide a direct coupling between the CFDC simulations of the turbulent fuel flow and the variable boundary conditions which arise from the buildup of deposits on the walls of fuel-injector feed-arms.

Formulation

Fluid flow, heat transfer, and deposit formation are treated by means of an integrated approach to simulate the time evolution of deposition inside heated tubes.

Chemical Kinetics

A simple global-chemistry kinetics model has been used to describe fuel degradation. The deposit-forming precursors in the fuel were assumed to be a separate species, along with the dissolved oxygen in this model. The crucial autoxidation reaction is modeled using a single irreversible reaction[4] as (reaction 1)

$$\text{fuel} + \text{oxygen} \Rightarrow \text{precursor}$$

In order to limit the concentration of precursors at higher temperatures (>500 K), another global reaction[5] (reaction 2)

$$\text{precursor} \Rightarrow \text{solubles}$$

has been added.

The high viscosity of the fuel causes a sublayer of very slowly moving fluid to form adjacent to the walls. The longer residence time associated with this fluid and other factors cause the autoxidation reaction (reaction 1) to underpredict the chemical reaction rate within this laminar sublayer. Therefore, another autoxidation reaction is included in the model as a wall reaction (reaction 3)

$$\text{fuel} + \text{oxygen} \Rightarrow \text{deposit}$$

The rates for reactions 1–3 are assumed to be governed by Arrhenius expressions.

The precursors formed within the fuel are transported to the wall surface as a result of convective fluid motion and molecular and turbulent diffusion processes. These precursors may stick to the wall surface and form deposits. Their sticking probability depends on several factors such as temperature, surface and precursor characteristics, and flow velocity. The lack of a fundamental understanding of the processes involved in sticking makes it difficult to obtain, from first principles, a functional form for the sticking phenomenon. Hence, in the present study, a simple model which considers only the homogeneity of the tube wall is proposed. This process is mathematically represented as a wall reaction (reaction 4)

$$\text{precursor} \Rightarrow \text{deposit}$$

The rate for this reaction is expressed as a function of deposit thickness as

$$\text{reaction rate} = A_4 \exp(-E_4/\Delta\text{Dep}) \tag{1}$$

where A_4 and E_4 are the pre-exponential and activation thickness, respectively. The deposit thickness ΔDep is the net result of deposition due to reactions 3 and 4.

Experiments conducted by Giovanetti[4] and Marteney[6] over long periods of time indicate that the deposition rate increases with exposure time. Since the clean fuel was driven throughout the testing period, these changes in deposition rate with exposure time may be attributed to changes in surface characteristics, deposit morphology, chemical reactions occurring near the wall, and the fluid dynamics within the test section (heat-transfer changes due to deposit buildup are negligible in this electrically resistance-heated experiment). Microscopic analysis revealed that the deposit surface is highly irregular and granular, and that the surface irregularity and structure of the cavities depend mainly on the fluid velocity and the deposit thickness. This rough surface, in turn, affects the deposit growth rate—less significantly by altering the surface sticking properties, but more significantly by trapping fuel and sucking it into the cavities. Since the fuel in the feed-arms flows at appreciable rates (velocities > 1 m/s), the deposits inside the tubes may be dense, as suggested by Marteney.[6] Also, the exposure times considered in the present study are not sufficiently long to result in thick deposits; therefore, reactions 1–4 in this analysis are assumed to be independent of morphological history of the deposit.

Governing Equations

Fluid motion inside the tube is assumed to be axisymmetric and is bounded by the fuel-deposit interface. Time-dependent Navier-Stokes equations along with turbulent-energy, species-conservation, and enthalpy equations are written in the z-r cylindrical coordinate system as follows:

$$\frac{\partial \rho}{\partial t} + \frac{\partial \rho u}{\partial z} + \frac{\partial (\rho v)}{\partial r} + \frac{(\rho v)}{r} = 0 \tag{2}$$

$$\frac{\partial (\rho \Phi)}{\partial t} + \frac{\partial (\rho u \Phi)}{\partial z} + \frac{\partial \rho v \Phi}{\partial r} = \frac{\partial}{\partial z}\left(\Gamma^{\Phi} \frac{\partial \Phi}{\partial z}\right) + \frac{\partial}{\partial r}\left(\Gamma^{\Phi} \frac{\partial \Phi}{\partial r}\right) - \frac{\rho v \Phi}{r} + \frac{\Gamma^{\Phi}}{r} \frac{\partial \Phi}{\partial r} + S^{\Phi} \tag{3}$$

Here ρ, u, and v are the density and the axial and radial velocity components, respectively. Equation (3) represents different conservation equations, depending on the variable assigned to Φ. The source terms S^{Φ} and the transport coefficients Γ^{Φ} associated with each of these equations are given in Table 1.

In the table, μ, κ, and c_p are the viscosity, thermal conductivity, and specific heat of the fuel, respectively, and μ_t is the turbulent viscosity incorporated through use of the k-ε turbulence model. The variables p, h, k, and ε are the pres-

Table 1 Source terms and transport coefficients appearing in governing equations

Φ	Γ^Φ	S^Φ
u	$\mu + \mu_t$	$-\frac{\partial p}{\partial z} + \frac{\partial}{\partial z}\left(\Gamma^u \frac{\partial u}{\partial z}\right) + \frac{\partial}{\partial r}\left(\Gamma^u \frac{\partial v}{\partial z}\right) + \frac{\Gamma^u}{r}\frac{\partial v}{\partial z}$
v	$\mu + \mu_t$	$-\frac{\partial p}{\partial r} + \frac{\partial}{\partial z}\left(\Gamma^v \frac{\partial u}{\partial r}\right) + \frac{\partial}{\partial r}\left(\Gamma^v \frac{\partial v}{\partial r}\right) + \frac{\Gamma^v}{r}\frac{\partial v}{\partial r} - 2\Gamma^v \frac{v}{r^2}$
k	$\mu + \frac{\mu_t}{\sigma_k}$	$G - \rho\varepsilon$
ε	$\mu + \frac{\mu_t}{\sigma_\varepsilon}$	$C_1 G \frac{\varepsilon}{k} - C_2 \rho \frac{\varepsilon^2}{k}$
h	$\frac{\kappa}{c_p} + \frac{\mu_t}{\sigma_h}$	0
Y_i	$\rho D_i + \frac{\mu_t}{\sigma_{Y_i}}$	$\dot{\omega}_i$

sure, enthalpy, and turbulence kinetic energy and its dissipation, respectively, and σ is the turbulent Prandtl number (or Schmidt number) associated with a specific transport equation. Y_i, $\dot{\omega}_i$, and D_i are the mass fraction, rate of production, and diffusion coefficient of the ith species, respectively. The other variables and constants appearing in the table are defined below:

$$G = \mu_t \left\{ 2\left[\left(\frac{\partial u}{\partial z}\right)^2 + \left(\frac{\partial v}{\partial r}\right)^2 + \left(\frac{v}{r}\right)^2\right] + \left(\frac{\partial v}{\partial z} + \frac{\partial u}{\partial r}\right)^2 \right\}$$

$$\mu_t = C_\mu \rho k^2/\varepsilon$$

$$C_1 = 1.47, \quad C_2 = 1.92, \quad \text{and} \quad C_\mu = 0.09$$

$$\sigma_k = 1.0, \quad \sigma_\varepsilon = 1.3, \quad \sigma_h = 1.0, \quad \text{and} \quad \sigma_{Y_i} = 1.0$$

Since a wide range of temperatures exists within the test section, the transport properties of the fluid vary significantly. A "typical" Jet-A fuel is used as the fluid in the present calculations, and the transport properties along with the enthalpy and density at the given temperature are obtained from the curve fits developed for Jet-A fuel.

For an accurate treatment of the boundary conditions, a body-oriented curvilinear coordinate system (Fig. 2) was used. The contravariant velocities and the inverse of the Jacobian associated with this ξ-η coordinate system are related to those of the z-r orthogonal system as follows:

$$U = \xi_z u + \xi_r v \tag{4}$$

$$V = \eta_z u + \eta_r v \tag{5}$$

$$J^{-1} = (z_\xi r_\eta - z_\eta r_\xi) \tag{6}$$

and the governing equations [Eqs. (2) and (3)] are rewritten as

$$\frac{\partial \rho}{\partial t} + \frac{\partial (J^{-1}\rho U)}{\partial \xi} + \frac{\partial (J^{-1}\rho V)}{\partial \eta} + \frac{J^{-1}}{r}(\rho v) = 0 \tag{7}$$

$$\frac{\partial (J^{-1}\rho\Phi)}{\partial t} + \frac{\partial (J^{-1}\rho U\Phi)}{\partial \xi} + \frac{\partial (J^{-1}\rho V\Phi)}{\partial \eta} = \frac{\partial}{\partial \xi}\left[J^{-1}(\xi_z^2 + \xi_r^2)\Gamma^\Phi \frac{\partial \Phi}{\partial \xi}\right] + \frac{\partial}{\partial \eta}\left[J^{-1}(\eta_z^2 + \eta_r^2)\Gamma^\Phi \frac{\partial \Phi}{\partial \eta}\right] - J^{-1}\frac{\rho v \Phi}{r} + J^{-1}\frac{\Gamma^\Phi}{r}\left(\xi_r \frac{\partial \Phi}{\partial \xi} + \eta_r \frac{\partial \Phi}{\partial \eta}\right) + \bar{S}^\Phi \tag{8}$$

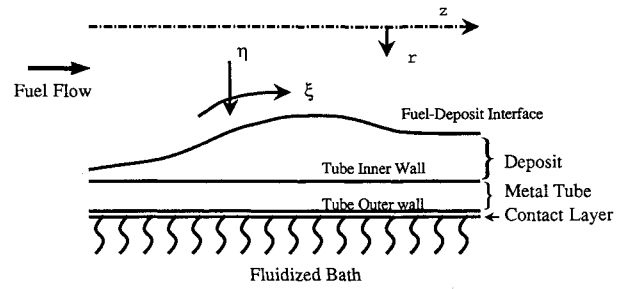

Fig. 2 Boundary segments and coordinate system used in calculations.

where

$$\bar{S}^\Phi = \frac{\partial}{\partial \xi}\left[J^{-1}(\xi_z\eta_z + \xi_r\eta_r)\Gamma^\Phi \frac{\partial \Phi}{\partial \eta}\right] + \frac{\partial}{\partial \eta}\left[J^{-1}(\xi_z\eta_z + \xi_r\eta_r)\Gamma^\Phi \frac{\partial \Phi}{\partial \xi}\right] + S^\Phi$$

Here the subscripts z and r indicate partial derivatives.

The governing equations [Eqs. (7) and (8)] are discretized utilizing a hybrid scheme[8] which is a second-order central-differencing scheme everywhere, but changes to a first-order upwind scheme when the local Peclet number $[(J^{-1})^2 U\Delta\xi/\Gamma^\Phi]$ becomes greater than two. An implicit approach is employed to advance the calculations using a large time-step (enabling the computation of several hours of real time to be made in a few minutes of computational time). After rearrangement of the terms, the finite-difference form of Eq. (8) for the variable Φ at a grid point P can be written into an algebraic equation as follows:

$$A_P^\Phi \Phi_P^{n+1} + A_{\xi^+}^\Phi \Phi_{\xi^+}^{n+1} + A_{\xi^-}^\Phi \Phi_{\xi^-}^{n+1} + A_{\eta^+}^\Phi \Phi_{\eta^+}^{n+1} + A_{\eta^-}^\Phi \Phi_{\eta^-}^{n+1} = \text{RHS} \tag{9}$$

Here, the subscripts ξ^+ and ξ^- indicate the values at the grid points immediately adjacent to point P in the positive and negative ξ directions, respectively. The coefficients A and the terms on RHS (right-hand side) are calculated from the known flow variables at the nth time step. The u and v momentum, k and ε turbulence, enthalpy, and the three species equations represented by Eq. (9) are solved individually using the alternate direction implicit (ADI) method. Finally, the pressure field is obtained through the use of the SIMPLE technique.[9]

The present formulation allows the deposit to grow on the wall surface. In other words, after each time-step the geometry of the fuel-deposit interface is allowed to change as part of the solution procedure. If Ω is the deposition rate in micrograms per square centimeter per hour, ρ_D is the deposit density in kilograms per cubic meter, and Δt is the time-step in hours, then the new fuel-deposit interface shape (r_{int}) is calculated from

$$r_{\text{int}}^{\text{new}} = r_{\text{int}}^{\text{old}} \sqrt{1 - (2\Omega\Delta t/10^3 \rho_D r_{\text{int}}^{\text{old}})} \tag{10}$$

The computational domain is bounded by the axis of symmetry and the fuel-deposit interface, and the grid system is reconstructed after each time step to take into account the changes in the boundary shape.

Boundary Conditions

The usual no-slip conditions are imposed at the fuel-deposit interface for the velocities. The normal derivative of a variable f at the boundary is written as

$$\frac{\partial f}{\partial n} = \frac{\xi_z\eta_z + \xi_r\eta_r}{\sqrt{\eta_z^2 + \eta_r^2}} f_\xi + \sqrt{\eta_z^2 + \eta_r^2} f_\eta \tag{11}$$

and is set equal to zero or a specified value, depending on the variable. With the use of central differencing in the ξ direction and first-order backward differencing in the η direction, Eq. (11) can be solved for the variable at the interface. The normal derivatives specified for different variables under laminar flow conditions are as follows:

Pressure

$$\frac{\partial p}{\partial n} = 0$$

Enthalpy

$$\frac{\partial h}{\partial n} = 0 \qquad \text{for adiabatic wall}$$

$$= \left(\frac{c_p}{\kappa}\right) \dot{q}_{\text{int}} \qquad \text{for constant heat flux}$$

$$T = T_{\text{int}} \qquad \text{for constant wall temperature}$$

Species

$$\frac{\partial Y}{\partial n} = \left(\frac{1}{\rho D_{O_2}}\right) \dot{\omega}_{O_2}|_{\text{int}} \qquad \text{for oxygen}$$

$$= \left(\frac{1}{\rho D_P}\right) \dot{\omega}_P|_{\text{int}} \qquad \text{for precursor}$$

Here, the subscript int represents the values at the fuel-deposit interface. The species production rates $\dot{\omega}_{O_2}$ and $\dot{\omega}_P$ are calculated from the wall reactions 3 and 4, respectively, and the heat flux $\dot{q}_{\text{int}}$ must be obtained by solving the heat-transfer equations for the deposit and the tube wall.

For the turbulent-flow conditions, wall functions[10] have been used to determine the variations of the flow variables near the fuel-deposit interface. Usually, wall functions relate the normal stresses (or the derivatives of the flow variables) in the Cartesian coordinate system at the wall to the k, ε values at a grid point inside the flowfield. Therefore, for the body-oriented curvilinear coordinate system, the wall functions proposed in Ref. 9 can be appropriately modified using Eq. (11).

Heat Transfer

The direct impact of deposits on heat exchangers is evident in the deteriorating heat-transfer characteristics. As deposits form on the wall surface, they offer resistance to the heat flow from the fuel in the tubes to the wall surface or vice versa. Therefore, complete definition of the problem necessitates solving for the heat distribution in the deposits and tube walls simultaneously with that of the flowing fuel. An analysis in the z-r coordinate system is presented for simplicity, although a similar approach in the ξ-η system was used in the actual calculations.

Since the deposit and tube-wall thicknesses are very small compared to the tube length, the heat equation for the heat flux can be written, after neglecting the heat conduction in the axial direction, as

$$\frac{\partial \dot{q}}{\partial r} + \frac{\dot{q}}{r} = 0 \tag{12}$$

The following analytical expressions for the heat-flux distributions in the deposit and the tube walls can be obtained by integration of the above equation:

$$\dot{q} = \dot{q}_o \frac{r_o}{r} = \dot{q}_{\text{wall}} \frac{r_{\text{wall}}}{r} = \dot{q}_{\text{int}} \frac{r_{\text{int}}}{r} \tag{13}$$

Here, the subscripts o and wall represent the outer and inner tube walls, respectively. If the thermal conductivities of the deposit and tube metal are denoted by κ_d and κ_t, respectively, their corresponding temperature distributions can be obtained by integrating

$$\dot{q} = \kappa \frac{dT}{dr} \tag{14}$$

as

$$T = T_{\text{int}} + \int_{r_{\text{int}}}^{r} \left(\frac{\dot{q}_{\text{int}} r_{\text{int}}}{\kappa_d}\right) \frac{1}{r}\, dr \tag{15}$$

$$T = T_{\text{wall}} + \int_{r_{\text{wall}}}^{r} \left(\frac{\dot{q}_{\text{wall}} r_{\text{wall}}}{\kappa_t}\right) \frac{1}{r}\, dr \tag{16}$$

If κ_t is independent of temperature, and the tube wall is assumed to have homogeneous properties, then an expression for the tube-outer-wall temperature can be obtained by solving Eq. (16) as

$$T_0 = T_{\text{wall}} + \frac{\dot{q}_{\text{wall}} r_{\text{wall}}}{\kappa_t} \ln\left(\frac{r_0}{r_{\text{wall}}}\right) \tag{17}$$

For the constant heat-flux boundary condition (i.e., for the given $\dot{q}_0$), at each time step, first Eq. (13) is solved for the value of $\dot{q}_{\text{int}}$, and then the fuel-flow calculations are performed using this value in the boundary condition described by Eq. (11). The given constant outer-wall-temperature condition can be implemented using the iterative procedure given below:

1) At a given axial location and time $t + \Delta t$, assume that the temperature at the fuel-deposit interface is equal to that at time t and calculate the heat flux $\dot{q}_{\text{int}}$ from the turbulent fuel-flow solution.

2) Obtain $\dot{q}_{\text{wall}}$ by solving Eq. (13).

3) Determine the tube-outer-wall temperature T_0 from Eq. (17); T_0 will be greater than the actual wall temperature because of the additional amount of deposition during Δt.

4) Now, relax the assumption made in step 1 to obtain a better value for the interface temperature and repeat steps 2 and 3; the entire procedure must be repeated until the calculated outer-wall temperature matches the specified value.

Results and Discussion

Evaluation of the Model

The mathematical model described above involves global-chemistry parameters which must be obtained, or calibrated, from well-controlled experiments for a given fuel. The global-reaction scheme (reactions 1–3) has been calibrated by Krazinski et al.[5] for a CFDC steady-state computational code using data from an electrically heated tube.[11] The pre-exponentials and the activation energies corresponding to each of these reactions are given in Table 2 under model A. The assumption of Krazinski et al.[5]—that the precursors transported near the wall stick to the wall instantaneously—may be treated in this model using a large value for the pre-exponential and zero for the activation thickness of the deposit-formation reaction (reaction 4).

For validation of the present code, which was developed based on the unsteady formulation, a short-duration experiment conducted by Marteney[11] was numerically simulated. Marteney[11] obtained deposition rates for a JP-5 fuel flowing through an electrically heated 2.25-mm-i.d. steel tube after a test time of <6 h. A fuel velocity of 2.12 m/s at the tube entrance triggered flow turbulence inside the tube. Calculations for this situation have been made using the reaction kinetics given by model A in Table 2. Perhaps the most sensitive parameter in deposit formation in the heated-tube ex-

Table 2 Rate constants and units used in global chemistry model

	Reaction 1		Reaction 2		Reaction 3		Reaction 4	
	$\frac{m^3}{mole\ s}$	$\frac{cal}{mole\ K}$	$\frac{1}{s}$	$\frac{cal}{mole\ K}$	$\frac{m^4}{mole\ s}$	$\frac{cal}{mole\ K}$	$\frac{m}{s}$	mm
Model A	1.0E + 08	30,000	3.0E + 15	35,000	6.34E − 08	8,000	1.0E + 20	0
Model B	3.0E + 08	27,000	1.0E + 18	40,000	6.34E − 08	8,000	1.0E + 20	0.1

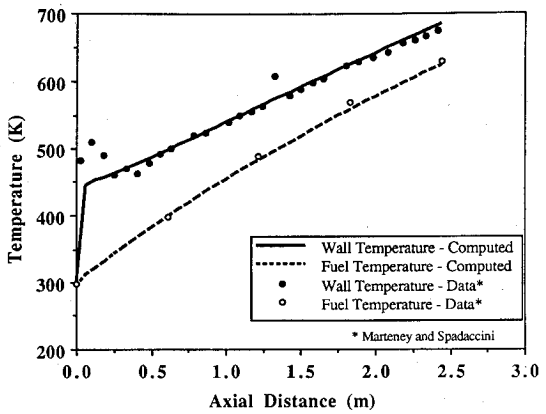

Fig. 3 Comparison of calculated and measured temperatures for constant heat-flux case.

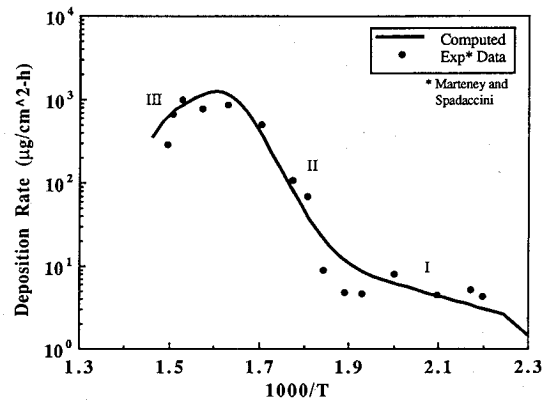

Fig. 4 Deposition rate computed with three-step global-chemistry reaction model.

periments is the wall temperature. Therefore, the numerical model to be used for thermal-degradation investigations should be first validated for its ability to predict wall temperature.

The wall and bulk-fuel temperatures along the tube length are shown in Fig. 3. The turbulence model and the wall functions used in the code accurately predicted these temperatures. The overshoot in the wall temperature near the tube entrance observed in the experimental data is due to the transition from laminar to turbulent flow. Since the code has no submodel for predicting the flow transition, calculations were made assuming a fully developed turbulent flow inside the tube. The deposition rate obtained by the code is plotted as a function of the inverse of temperature in Fig. 4 along with the experimental data. The global-chemistry model was partially calibrated[5] for this experiment. The computed deposition-rate curve closely follows the experimental data. The portion of the curve in the lower temperature range marked "I" in Fig. 4 is caused by the wall autoxidation reaction 3. In the moderate temperature regime (segment II), the bulk-fuel autoxidation reaction 1 is dominant. The impact of the precursor-controlling reaction 2 can be seen in Fig. 4 along the descending portion (segment III) of the deposition-rate curve.

Simulations for the Injector Feed-Arm

The next goal of the present study was to determine how well the numerical model described above would predict

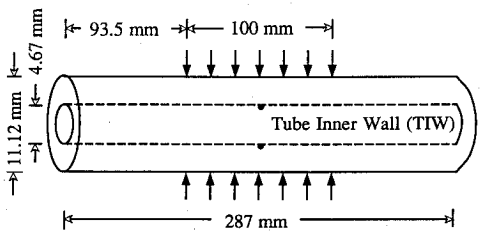

Fig. 5 Schematic diagram of model feed-arm used by Kendall et al.[12]

deposition in a more practical system. Kendall et al.[12] studied experimentally the fouling characteristics of a model gas-turbine injector feed-arm. Recently, Clark and Stevenson[13] conducted experiments on a half-scale model of the feed-arm under very similar thermal-stressing conditions in order to understand the effects of scaling on fouling. Both studies indicate three distinct phases of the deposition process. Insignificant deposition occurs during the initial "induction period," followed by a near-constant rate of deposition over a long period; in some cases, a decrease in deposition rate was observed near the end of the test. The initial low deposition rate during the induction period is generally thought to be a result of the initial clean tube surface. The activation thickness [Eq. (1)] in the present model may be related to the experimentally observed induction period. It should be noted that the fuels used by Kendall et al.[12] and Clark and Stevenson[13] are not the same fuels used in the experiments of Marteney,[11] for which the global-chemistry model was calibrated. Thus, it might be expected that the difference in fuels would make some changes in the pre-exponential and activation energies in the global-chemistry model.

Full-Scale Tests

The feed-arms were designed[12] to simulate the burner tubes leading to the nozzles of a large gas turbine. These are straight, thick-walled tubes (Fig. 5) of 4.76-mm bore. The central 100-mm section of the feed-arm was immersed in a fluidized bath. The aviation fuel (Jet A), preheated to a bulk temperature of 438 K, was pumped through the feed-arm at flow rates of 72 and 36 kg/h. The temperature of the fluidized bath was 813 K which resulted in a temperature of 573 K at the inner wall of the tube (TIW). Tests were conducted for time periods of up to 80 h, and changes in the tube inner-wall temperature (ΔTIW) were monitored as a function of time.

Numerical simulations were first made for the higher-flow-rate case (identified as case 1), i.e., 72 kg/h, which corresponds to a 1.5-m/s flat velocity (Re = 25,034) at the tube entrance. The fluidized-bath temperature was set at 813 K to match the temperature used in the experiments. Since the fluidized bath around the tube does not make perfect contact with the tube outer wall, a temperature drop occurs across a thin layer between the fluidized bath and the tube. This is treated as a contact layer (cf. Fig. 2) in the simulations. Turbulent-flow and heat-transfer calculations were carried out initially without activating the chemical reactions within the bulk fuel or on the wall surface. The resistance of the contact layer was adjusted in such a way that the temperature at TIW (Fig. 5) would be 438 K. Once the initial fuel flow was established, the unsteady calculations were performed using the reaction-rate constants of model A (see Table 2) which was calibrated for a constant-heat-flux experiment. After each 1-min time step, the amount of deposit on the tube wall was

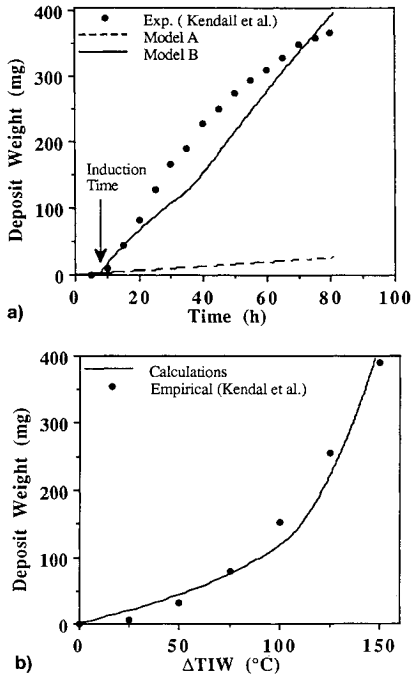

Fig. 6 Results for case 1: a) calculated and measured deposition at different times during 80-h test (used for calibration), and b) relationship between amount of deposition on tube walls and associated rise in ΔTIW.

calculated by integrating the deposition over the entire tube length. A deposit density of 1 gm/cm^3 was used. This value was determined experimentally by Marteney[6] under similar velocity conditions. The value of 0.1 W/m°C used for the thermal conductivity of the deposit is close to that of ~0.16 W/m°C found by Goodman and Bradley.[14]

The total weight of the deposit collected on the tube inner wall at different exposure or run times up to 80 h is plotted in Fig. 6a (broken line); measured values obtained by Kendall[12] are also plotted in this figure (solid circles). The very small amount of deposition predicted by the model indicates that the global-reaction scheme calibrated for the JP-5 fuel used by Marteney[11] was not applicable for the present feed-arm experiment. Therefore, the global-chemistry model was recalibrated for the Jet-A fuel by repeating the calculations, choosing different values for the pre-exponentials and activation energies for reactions 1–4. The calculated deposition weights which best fit the experimental data are shown in Fig. 6a, and the constants associated with reactions 1–4 are given in Table 2 under model B. The value of 0.1 mm used for the activation thickness appears to be sufficient for reproducing the observed induction period. The differences in the shapes of the measured and calculated deposition curves indicate the limitations of the global-chemistry model.

Kendall et al.[12] obtained the weight of the deposit by an indirect method. For each flow condition, a few specific experiments were conducted using different run times. The information on the change in the ΔTIW and the weight of the deposit measured at the end of each run was recorded and later used to obtain an empirical relation between the deposit weight and ΔTIW. In the actual deposition experiments, only ΔTIW was measured and the deposit weight was obtained using the predetermined empirical relation. Figure 6b shows the computed ΔTIW due to deposition for case 1. The empirical relation for this flow rate determined by Kendall et al.[12] is $W_D = 0.00367^*(\Delta TIW)^{2.31}$, and the data obtained from this relation are plotted in Fig. 6b (solid circles). After 80 h of exposure, the tubes accumulated ~400 mg of deposit; as a result, the inner-wall temperature at the center of the tube changed by ~150°C. This clearly indicates the severe effect of fouling on heat transfer in a tube surrounded by a fluidized bath. The good agreement between calculated and experimental results demonstrates the ability of the present model to predict the changes in heat transfer due to deposition.

Effect of Velocity

The deposit weight as a function of time measured by Kendall et al.[12] at a fuel flow rate of 36 kg/h and a fuel velocity of 0.75 m/s (identified as case 2) is plotted in Fig. 7a (solid circles). One might expect that because the fuel velocity in case 2 is lower than that in case 1, the deposition rate would be higher for case 2 since the fuel residence time in the tube is longer. Direct comparison of the experimental data in Figs. 6a and 7a indicates that this is not the case. The measured deposition rate actually decreased with fuel velocity.

The calibrated model was used to predict deposit weight as a function of test time under case 2 conditions. The calculated results are plotted in Fig. 7a. The induction time did not change appreciably with velocity, and good agreement is observed between predicted and measured values. In fact, the calculations also show a reduction in deposition rate compared to that of the higher velocity case. The value of a CFDC-based model is that it can be used to examine why the deposition rate decreases with fuel velocity. For both flow rate cases, the inlet-fuel temperature and the initial TIW were maintained identical. An examination of the model data showed that the bulk-fuel temperatures were higher under case 2 than under case 1 conditions. This is true, because at lower velocity the fuel in case 2 spends more time in the tube and thereby receives more heat from the wall surface which was maintained at a temperature of 573 K in both cases. The higher fuel temperatures in case 2 decreased the precursor concentration due to reaction 2, which converts precursors to soluble products. This results in a lower deposition rate, as compared to that in case 1. This simple explanation is only as good as the global-chemistry model used in the CFDC calculations. However, it illustrates the potential of the model for exploring the physical and chemical processes which might explain otherwise confusing results.

The model has provided an explanation that can be examined directly in future experiments. Reaction 2 was introduced into the global-chemistry model for deposition[5] to take into account two experimental observations:[11] 1) the deposition rate decreases at higher temperatures, and 2) an appreciable amount of oxygen is still present at those temperatures. These observations were made on a particular JP-5 fuel. How-

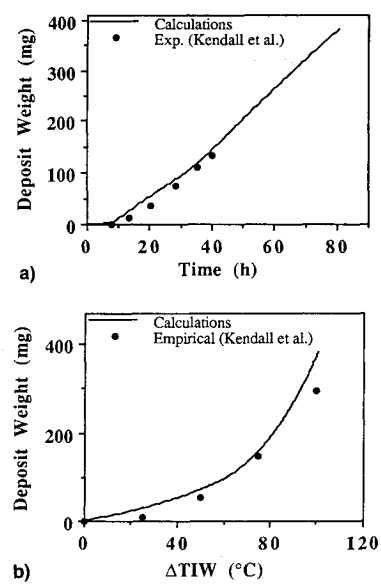

Fig. 7 Results for case 2: a) comparison of predicted and measured deposit weights, and b) comparison of calculated and experimental relationships between amount of deposition on tube walls and associated rise in tube-inner-wall temperature.

ever, recent experiments on heated tubes by Heneghan[15] and Jones[16] with different fuels indicate that the oxygen inside the tubes has been consumed by the time the fuel has attained a temperature of 460 K; they attribute the decrease in deposition at higher temperature to the depletion of oxygen in the fuel. In such fuels, reaction 2 may be overwhelmed by reaction 1, and the present model cannot predict higher deposition rates with an increase in fuel velocity. The calibrated global-chemistry model for Jet-A fuel used in the feed-arm experiment predicts that the dissolved oxygen will not be totally consumed and that a considerable amount of oxygen will remain in the outgoing fuel. In order to validate the model, additional measurements for species such as dissolved oxygen should be made in future experiments. Despite the outcome of such an examination, the model predictions clearly indicate that the heat-transfer effects overcome the chemical effects expected from a longer residence time and, in turn, cause a decrease in the deposition rate.

For the lower flow rate (case 2), the deposit weight and ΔTIW were found[12] to be related by the empirically derived expression $W_D = 0.00407*(\Delta TIW)^{2.43}$. Values obtained from this relation are shown in Fig. 7b along with those prediced by the model. A comparison with the results in Fig. 6b show that for the same deposit weight (or deposit thickness), the temperature change at the inner wall (ΔTIW) is larger for the higher flow rate case, which means that the effects of deposition on heat-transfer characteristics will increase with increasing fuel flow rate or, conversely, decrease with decreasing fuel flow rate.

Half-Scale Tests

A half-scale apparatus having a feed-arm tube similar in length to the full-scale tube sketched in Fig. 5 and operating at identical temperatures was designed by Clark and Stevenson[13] to reduce the amount of fuel required for their experiment. The wall thickness of the half-scale tube is 2.032 mm, and the bore is 2.286 mm. Jet-A aviation fuel, preheated to 438 K, passed through the tube at a rate of 300 ml/min, which corresponds to a mass-averaged velocity of 1.218 m/s (Re = 9950). The fluidized-bath temperature in the calculations (identified as case 3) was set equal to 700 K, a value chosen in the range 683–723 K used in the experiments. The contact resistance was then adjusted to obtain the specified clean-tube inner-wall temperature (TIW) of 573 K at the midsection.

The computed and measured deposit weights at different exposure times are plotted in Fig. 8a. The deposit weight

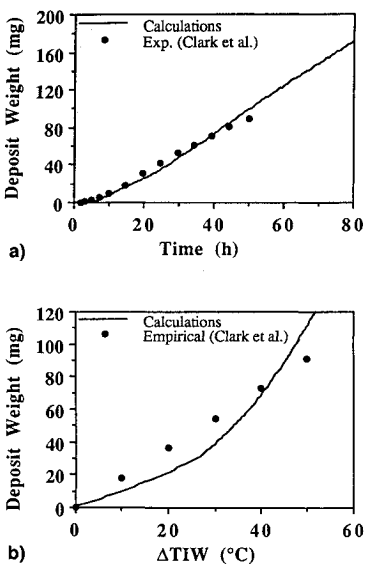

Fig. 8 Results for half-scale feed-arm rig (case 3): a) calculated and measured deposits, and b) calculated and experimentally observed relationships between amount of deposit and associated ΔTIW.

increased very slowly (0.0132 mg/cm²/h) up to 6–7 h and, thereafter, rapidly at a rate of 0.275 mg/cm²/h. Induction time in the calculations was modeled using an activation thickness of 0.1 mm in Eq. (1). When the tube is clean, deposition on the wall surface occurs as a result of the wall reaction only. On the fouled surface, the deposition rate approaches that given by the bulk reactions in an exponential manner. This is analogous to the argument[13] that the reciprocal induction period is a measure of fuel-deposition rate on a clean metal surface, whereas the postinduction rate is a measure of the deposition rate on a fouled surface. The good agreement obtained for the calculated and measured induction times (Fig. 8a) supports this idea.

Changes in the TIW with deposition weight are plotted in Fig. 8b. The computations show a nonlinear relationship between ΔTIW and the amount of deposit. Clark and Stevenson[13] observed that a linear relationship fit the data (not shown in their paper), and speculated that the difference in the fluidized-bath temperatures for the full-scale and half-scale rigs could result in changes in heat-transfer characteristics between the fluidized bath and the feed-arm and, hence, in relationships between ΔTIW and deposit weight. This is not the case, because the temperature drop across the solid deposit is always a logarithmic function of deposit thickness. However, in case 3, the temperature drop per unit thickness of deposit could be sufficiently small that a linear approximation of the logarithmic behavior might be reasonable. This idea is supported by the following two observations:

1) The temperature drop across the deposit in case 3 is only 47.5°C as compared to those of 124 and 82°C for cases 2 and 3, respectively.

2) Although the rate of deposition is low in case 3 as compared to that observed in either case 1 or case 2, the deposit thickness at 50 h of test time is approximately the same for all three cases because of the difference in innertube radii. This implies that the relatively slow temperature drop with deposition in case 3 results in a linearizing effect on the empirical curve fits.

Details Along the Tube Length

In the previous sections, computed results were presented in the form of total deposits accumulated inside the tube and the temperature changes at the inner wall of the midsection; these results compared favorably with the experimental data. In this section details along the tube length are discussed.

Since the temperature inside the tube is not uniform, the growth of deposits on the tube wall surface will be uneven. The location of the fuel-deposit interface along the length of the tube is shown in Fig. 9a. At time $t = 0$ this interface coincides with the tube-inner-wall surface. Although only the 0.1-m central section was heated by the fluidized bath, the flow of hot fuel before and after the heated section caused fouling on these sections as well. Deposit growth at the center of the tube ($z = 0.1435$ m) is less during the 40–80 h period than during the 0–40 h period. This reduction in deposition for longer times was also observed by Clark and Stevenson[13] and is due to the insulating effect of the cumulative deposit, as can be seen in Fig. 9b where the instantaneous deposition rates at three different times are plotted. The rate of deposition at the center at 80 h is lower than that at 40 h. At time $t = 0$, the deposition rate is very low along the entire length of the tube, corresponding to the wall autoxidation reaction 3 only. The induction submodel in the present study prevents precursors formed within the bulk fuel from sticking on the wall surface at this time. The lower wall temperature of the preheater section (438 K) yields a clean-tube deposition rate which is lower than that at the midsection. As a result, the induction period in this section extends beyond 40 h. This effect of temperature on induction period may be viewed as the tendency of fuels having lower thermal stability to exhibit shorter induction periods.

Heat and fuel flow are visualized in Fig. 10 in the form of isotemperature and isoturbulent energy contours beyond 80

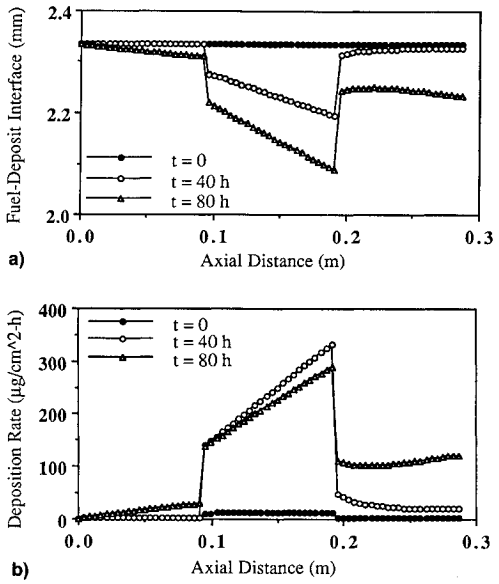

Fig. 9 Changes in a) deposit-fuel interface geometry and b) deposition rate at different axial locations after 40 and 80 h.

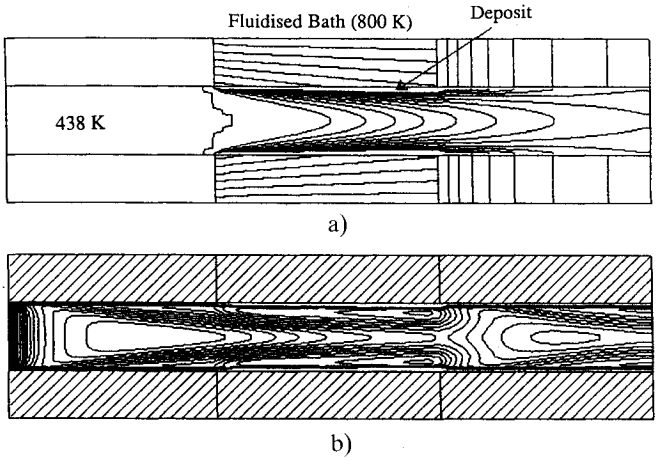

Fig. 10 Flow and heat distributions at the end of 80-h test on full-scale rig: a) temperature within tube wall and fuel and b) turbulent kinetic energy.

h. Deposits on the tube wall are also shown in these figures between the inner-wall surface and the contour lines in the fuel. Because of the adiabatic wall conditions imposed on the preheater section, both the fuel and tube wall are at the same temperature which, in this case, is identical to that of the inlet fuel (438 K). As fuel passes through the heater section, its temperature increases, as evidenced by the parabolic contours in the temperature field. The temperature distribution within the tube wall is dependent on the heat flux entering into the fuel at any cross section. The heat flux will be at a maximum at the entrance section of the heated zone and at a minimum at the exit section. In the postheater portion of the tube, equilibration of the fuel temperature results in a decrease in temperature at the tube-inner-wall surface. Again, because of the adiabatic wall conditions used in this section, a uniform temperature is obtained within the wall at an axial location.

Deposit growth not only affects the heat transfer, but also blocks the fuel flow. Uneven deposition along the tube wall is evident in Fig. 9a. The blockage (percentage ratio of blocked to clean-tube area) gradually increases in the heater section, reaching a maximum of ~20% near the tube end. This contraction causes fuel inside the tube to accelerate, resulting in a higher turbulent energy, as indicated by the closed isoenergy contours (Fig. 10b) near the deposition. The sudden expansion resulting from a decrease in blockage from 20 to 7.7% immediately after the heater section relaxes the turbulent energy, as shown by the diverging contours. The actual velocity distribution along the centerline is plotted in Fig. 11a. Calculations were initiated with a flat velocity profile at the entrance of the tube. As the fuel flows through the preheater section, a fully developed turbulent velocity profile is established, and the centerline velocity levels off at a value of 1.94 m/s just before the heater section. Within the heater section, wall heating causes the fuel nearer the wall to become hotter than that at the center. The lower density and viscosity of the higher temperature fuel accelerates the flow near the wall which, in turn, reduces the fuel velocity at the center (seen as a valley in the velocity distribution) (Fig. 11a) at $t = 0$. At all other times $t > 0$, the centerline velocity increases with the blockage. Interestingly, just after the heater section, the velocity of the fuel at the centerline actually decreases. Expansion around the backward-facing step-type deposit geometry creates vorticity in that region.

The temperature distribution at different boundaries along the tube length is shown in Fig. 11b for three instants of time. When the tube is clean (i.e., at $t = 0$), the fuel-deposit interface becomes the fuel-inner wall interface. As the exposure time increases, the deposits accumulate on the inner wall, and a temperature drop develops across the deposit; this drop is actually shared by the fuel and the tube wall. The temperature at the inner wall increases, approaching the fluidized bath temperature; at the fuel-deposit interface, it decreases, approaching the inlet-fuel temperature. After 80 h the temperature of the inner wall at the midsection ($z = 0.1435$ m) is 722 K—a rise of 149°C from the initial temperature. This compares favorably with the measured ΔTIW of 150°C. On the other hand, the temperature at the fuel-deposit interface has decreased by 84°C. The insulation effect of the deposit is evident in the bulk-fuel temperature plot (Fig. 11c). Because of the high flow rate (72 kg/h) and short heater section, the fuel temperature increased by only 11°C when the tube was clean and by only 4°C near the end of the experiment.

Deposition occurs in heated tubes primarily as a result of temperature. The presence of deposits changes the heat-transfer characteristics and blocks the tube. Heat usually comes into the fuel from the outside environment after passing through several layers of resisting materials. Any computational method designed to predict deposition should be accurate in treating this complex transfer of heat. The present formulation with a body-oriented coordinate system and an iterative method used to link the fluid flow and boundary calculations is very effective in solving this problem. The accuracy of the calculations may be validated by comparing the amount of heat energy supplied to the system with that actually present in the fuel.

The heat energy available in the fuel in a given cross section ($z = L$) may be obtained by mass averaging the local enthalpy as

$$h_{\text{fuel}} = h_{\text{in}} + \frac{1}{\dot{m}} \int_0^{r_{\text{int}}} (2\pi r)\rho u h \, dr \qquad (18)$$

Similarly, the heat energy supplied to the section at $z = L$ is calculated by integrating the heat flux at the outer wall and is given by

$$h_{\text{supplied}} = h_{\text{in}} + \frac{(2\pi r_o)}{\dot{m}} \int_0^{L} (\dot{q}_o) \, dz \qquad (19)$$

The supplied and available energy distributions along the axial distance are compared in Fig. 11d at time $t = 0$ and at the conclusion of the test. The heat energy increased linearly in the clean heater section; since no losses are incorporated into the model, this energy remained constant in the other sections. The small discrepancy between the supplied and available energy is mainly due to the error involved in the numerical integration of Eq. (18). The heating efficiency (per-

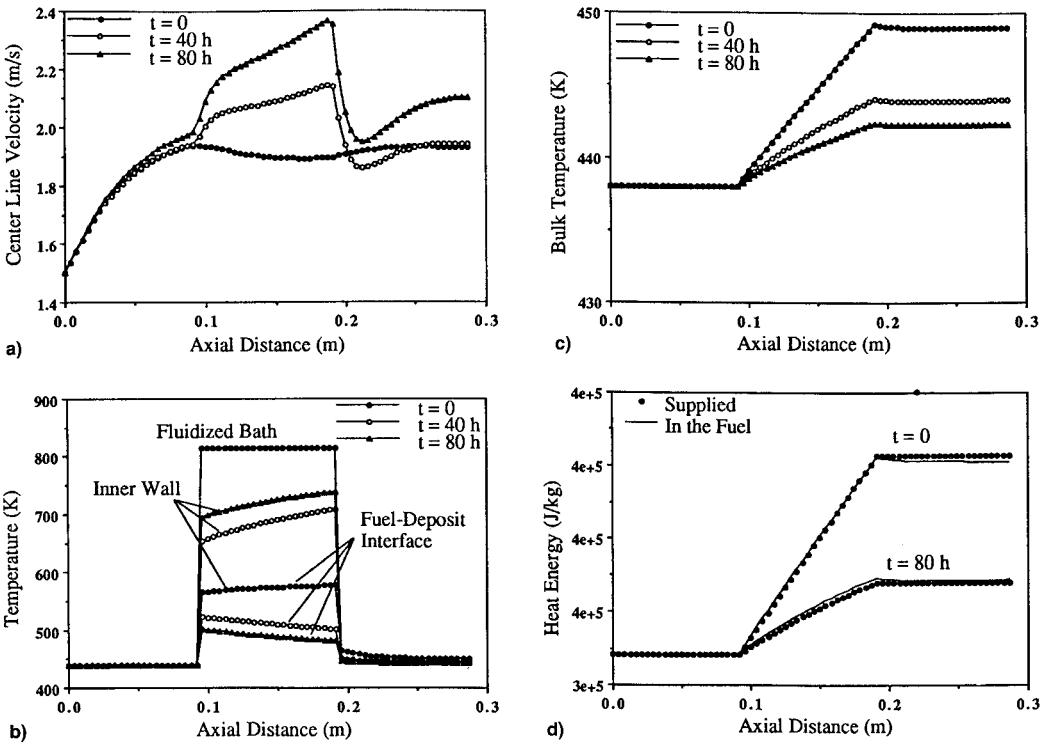

Fig. 11 Effect of deposition on a) fuel velocity, b) temperature at different interfaces, c) bulk-fuel temperature, and d) added and available heat energies.

centage ratio of heat energy received at a particular time to that received when the tube was clean) of the rig has been reduced to 36.6% by the end of the 80th hour. As mentioned earlier, the blockage to the fuel flow at this instant was 20%. On the other hand, in the half-scale rig (case 3) the blockage was 30%, but the heating efficiency remained at 46.6%.

Conclusions

A numerical method for simulating deposit growth inside a fuel-injector feed-arm has been presented. The global-chemistry model calibrated for a series of electrically resistance-heated tubes failed to generate deposits in the feed-arms. This is thought to be due to the difference in the fuel used in the electrically heated tube and that used in the feed-arm experiments. Bulk reaction rates were recalibrated to correlate the predicted deposition with the measured data for an experiment conducted on the full-scale feed-arm rig. The induction period observed in the deposition growth was mathematically treated by introducing a wall-reaction-type mechanism for sticking. An activation thickness of 0.1 mm was sufficient to reproduce the measured induction time. Through use of the same chemistry, simulations were made for a half flow rate case on a full-scale rig and a quarter flow rate case on a half-scale rig. Good agreement was obtained for both deposit growth and temperature changes. The flow rate appeared to have no direct effect on deposition; however, the heat-transfer changes resulting from the flow rate perturb deposit growth. It was observed in the present study that in identical thermal environments 1) the impact of fouling on heat-transfer is less at lower fuel flow rates, and 2) blockage to the fuel flow is less for larger tube bores. Present calculations in fairly uniform temperature environments and earlier calculations in a tube where the temperature was rapidly increasing, suggest that deposition depends strongly on wall temperature and weakly on bulk-fuel temperature. Recent experimental studies on the "Phoenix Rig"[15] lend support to this concept. The four-step global-reaction model used in the current study lacks this important element. Development efforts on the next-generation global-reaction model for deposition will be based on the vast amount of data being gathered from the Phoenix Rig.

Thermal decomposition of fuel is the result of highly complex chemical kinetics which depend not only on the type of fuel, but also on the batch. Development of a mathematical model for predicting the deposition process inside heated tubes based on elementary reactions is, therefore, not feasible in the near term. The fouling problem is further complicated by the lack of fundamental understanding of the surface sticking phenomenon. The global-chemistry models proposed in Ref. 5 and in this article seem promising for predicting performance deterioration due to fouling; however, such models must be calibrated a priori for the given fuel. Until recently, such calibration was made using the data obtained in flowing experiments. A more scientific approach to the problem would be to calibrate the global-chemistry model using data collected from quick static experiments. Future work should be focused on designing simple experiments which can be utilized to improve the chemistry and sticking models.

Acknowledgments

This work was supported, in part, by U.S. Air Force Contract F33615-90-C-2033. V. R. Katta acknowledges NRC and AFSC for sponsoring him under the Postdoctoral Fellowship Program during 1989–91. The authors would like to thank Marian Whitaker, Royce Bradley, Donn Storch, and Tim Edwards for their helpful comments.

References

[1]Koff, B. L., "The Next 50 Years of Jet Propulsion, the Global Anniversary of Jet Powered Flight: 1939–1989," Dayton and Cincinnati AIAA Meeting, Dayton, OH, Aug. 1989.

[2]"CRC Literature Survey on the Thermal Oxidation Stability of Jet Fuel," Coordinating Research Council Rept. 509, Atlanta, GA, April 1979.

[3]Deshpande, G. V., Serio, M. A., Solomon, P. R., and Molhotra, R., "Modeling of the Thermal Stability of Aviation Fuels," *Preprints from the Symposium on the Chemical Aspects of Hypersonic Propulsion*, American Chemical Society, Div. of Petroleum Chemistry, Miami, FL, Vol. 34, No. 3, 1989, p. 955.

[4]Giovanetti, A. J., and Szetela, E. J., "Long Term Deposit Formation in Aviation Turbine Fuel at Elevated Temperature," AIAA 24th Aerospace Sciences Meeting, AIAA Paper 86-0525, Reno, NV, Jan. 6–9, 1986.

[5]Krazinski, J. L., Vanka, S. P., Pearce, J. A., and Roquemore, W. M., "A Computational Fluid Dynamics and Chemistry Model for Jet Fuel Thermal Stability," *Journal of Engineering for Gas Turbines and Power*, Vol. 114, Jan. 1992, pp. 104–110.

[6]Marteney, P. J., "Thermal Decomposition of JP-5 in Long Duration Tests," Naval Propulsion Center, TR NAPC-PE-201C, Trenton, NJ, 1988.

[7]Reddy, K. V., and Roquemore, W. M., "A Time-Dependent Model with Global Chemistry for Decomposition and Deposition of Aircraft Fuels," *Preprints from the Symposium on the Stability and Oxidation Chemistry of Middle Distillate Fuels*, American Chemical Society, Washington, DC, Aug. 1990.

[8]Spalding, D. B., "A Novel Finite Difference Formulation for Difference Expressions Involving Both First and Second Derivatives," *International Journal for Numerical Methods in Engineering*, Vol. 4, No. 4, 1972, pp. 551–559.

[9]Patankar, S. V., and Spalding, D. B., "A Calculation Procedure for Three-Dimensional Parabolic Flows," *International Journal of Heat and Mass Transfer*, Vol. 15, Oct. 1972, pp. 1787–1805.

[10]Launder, B. E., and Spalding, D. B., "The Numerical Computation of Turbulent Flows," *Computer Methods in Applied Mechanics and Engineering*, Vol. 3, No. 2, 1974, pp. 269–289.

[11]Marteney, P. J., and Spadaccini, L. J., "Thermal Decomposition of Aircraft Fuels," *Journal of Engineering for Gas Turbines and Power*, Vol. 108, Oct. 1986, pp. 648–653.

[12]Kendall, D. R., Houlbrook, G., Clark, R. H., Bullock, S. P., and Lewis, C., "The Thermal Degradation of Aviation Fuels in Jet Engine Injector Feed-Arms: Part 1—Results from a Full-Scale Rig," 30th International Gas Turbine Congress, Tokyo, Oct. 1987.

[13]Clark, R. H., and Stevenson, P. A., "The Thermal Degradation of Aviation Fuels in Jet Engine Injector Feed-Arms: Results from a Half-Scale Rig," *Preprints from the Symposium on the Stability and Oxidation Chemistry of Middle Distillate Fuels*, American Chemical Society, Washington, DC, Aug. 1990.

[14]Goodman, H., and Bradley, R., "High Temperature Hydrocarbon Fuels Research in an Advanced Aircraft Fuel System Simulator," Air Force Aero Propulsion Lab. TR-70-13, Wright-Patterson AFB, OH, March 1970.

[15]Heneghan, S. P., Martel, C. R., Williams, T. F., and Ballal, D. R., "Studies of Jet Fuel Thermal Stability in a Flowing System," International Gas Turbine and Aeroengine Congress and Exposition, American Society of Mechanical Engineers Paper 92-GT-106, Cologne, Germany, June 1–4, 1992.

[16]Jones, E. G., and Balster, W. J., "Application of a Sulphur-Doped System to the Study of Thermal Oxidation of Jet Fuels," International Gas Turbine and Aeroengine Congress and Exposition, American Society of Mechanical Engineers Paper 92-GT-122, Cologne, Germany, June 1–4, 1992.